




# Impact of formation process on the radiation properties of single-photon sources generated on SiC crystal surfaces

Cite as: Appl. Phys. Lett. **118**, 204005 (2021); <https://doi.org/10.1063/5.0048772>

Submitted: 26 February 2021 . Accepted: 30 April 2021 . Published Online: 21 May 2021

 Yasuto Hijikata, Shota Komori, Shunsuke Otojima,  Yu-Ichiro Matsushita, and  Takeshi Ohshima

## COLLECTIONS

Paper published as part of the special topic on [Non-Classical Light Emitters and Single-Photon Detectors](#)



View Online



Export Citation



CrossMark

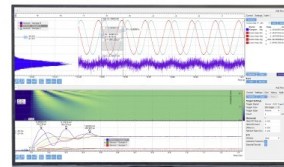
## ARTICLES YOU MAY BE INTERESTED IN

[Carrier dynamics of silicon vacancies of SiC under simultaneous optically and electrically excitations](#)

Applied Physics Letters **118**, 021106 (2021); <https://doi.org/10.1063/5.0028318>

Challenge us.

What are your needs for periodic signal detection?



Zurich Instruments

# Impact of formation process on the radiation properties of single-photon sources generated on SiC crystal surfaces

Cite as: Appl. Phys. Lett. **118**, 204005 (2021); doi: [10.1063/5.0048772](https://doi.org/10.1063/5.0048772)

Submitted: 26 February 2021 · Accepted: 30 April 2021 ·

Published Online: 21 May 2021



View Online



Export Citation



CrossMark

Yasuto Hijikata,<sup>1,a)</sup>  Shota Komori,<sup>1</sup> Shunsuke Otojima,<sup>1</sup> Yu-Ichiro Matsushita,<sup>2</sup>  and Takeshi Ohshima<sup>3</sup> 

## AFFILIATIONS

<sup>1</sup>Graduate School of Science and Engineering, Saitama University, Saitama 338-8570, Japan

<sup>2</sup>Tokyo Tech Academy for Convergence of Materials and Informatics, Tokyo Institute of Technology, Yokohama 226-8503, Japan

<sup>3</sup>Quantum Beam Science Research Directorate, National Institutes for Quantum and Radiological Science and Technology, Gunma 370-1292, Japan

**Note:** This paper is part of the APL Special Collection on Non-Classical Light Emitters and Single-Photon Detectors.

<sup>a)</sup>Author to whom correspondence should be addressed: [yasuto@opt.ees.saitama-u.ac.jp](mailto:yasuto@opt.ees.saitama-u.ac.jp)

## ABSTRACT

Radiation centers that are generated on the surface of SiC crystals [surface single-photon sources (SPSs)] have received much attention because they behave as high-brightness SPSs at room temperature. However, little is known about surface SPSs, such as their defect structure and radiation properties. To achieve a better understanding of surface SPSs, we investigated the impact of the formation processes of SPSs on the radiation properties. Low temperature photoluminescence (PL) measurements indicated that the photon energies of the zero-phonon line (ZPL) were dispersed in the range of 0.33 eV. In comparison between the (0001) Si-face and (11–20) *a*-face, the energy dispersion for the *a*-face was smaller, which suggests that the energy dispersion was attributed to stacking faults at the oxide–SiC interface. The differences in the radiation properties of the surface SPSs were clarified according to the formation process in terms of the oxide thickness and post-oxidation Ar annealing. The results showed that the wavelength dispersion was increased with the oxide thickness, and Ar annealing caused various changes in the radiation properties, such as a reduction in the density of SPSs, and the radiation intensity of the ZPL as well as a shift in the ZPL wavelength. Notably, most of the changes in the defect structure occurred at the Ar anneal temperature of 600 °C, and we discuss some of the types of defects that change at this temperature.

© 2021 Author(s). All article content, except where otherwise noted, is licensed under a Creative Commons Attribution (CC BY) license (<http://creativecommons.org/licenses/by/4.0/>). <https://doi.org/10.1063/5.0048772>

Single defects in widebandgap semiconductors have recently been utilized as single-photon sources (SPSs) to realize a light source for quantum encrypted communication capable of extremely high security, or quantum sensors that have made possible extremely high sensitivity and resolution magnetic field or temperature measurements.<sup>1</sup> An SPS generally emits one characteristic photon which has an energy that corresponds to the highest-occupied-molecular orbital (HOMO)–lowest-unoccupied-molecular orbital (LUMO) gap, while an electron at the excited state transits to the ground state. At present, quantum dots<sup>2</sup> and nitrogen vacancy (NV) centers in diamond<sup>3</sup> have been proposed as SPSs. However, quantum dots require cryogenic temperatures to obtain sufficient generation rates. Although NV centers in diamond emit photons with a high generation rate at room temperature, some issues remain in the device fabrication processes.

Silicon carbide (SiC) is one of the most promising candidates to meet all of the aforementioned requirements. The crystal growth technology of SiC has been developed with the introduction of mass-produced large-scale wafers. In addition, there have been many achievements in device fabrication technologies, especially in the development of power devices. SPSs in SiC, such as Si vacancies ( $V_{Si}$ ),<sup>4–6</sup> Si and C vacancy pairs ( $V_{Si}V_C$ ),<sup>7</sup> and carbon antisite-vacancy pairs ( $C_{Si}V_C$ ),<sup>8</sup> have been identified to date. In addition to these SPSs, it has been reported that surface SPSs were formed on the crystal surface simply by the oxidation of SiC substrates for several minutes.<sup>9</sup> The surface SPS has some advantages to realize a practical single-photon emitting device with characteristics, such as high brightness of more than twice the single-photon generation rate of NV centers in diamond and the ability to electrically control the single-photon emission.<sup>10–12</sup> However,

TABLE I. Substrates used in this study.

Substrate #	Polytype	Surface orientation	Off-cut angle (°)	Epilayer thickness ( $\mu\text{m}$ )	Carrier concentration ( $\text{cm}^{-3}$ ) (All $n$ -type)
#1	4H	Si-face	4	5.0	$8.4 \times 10^{15}$
#2	6H	Si-face	3.5	4.9	$5.0 \times 10^{15}$
#3	6H	$a$ -face	...	N/A	Unknown
#4	4H	Si-face	4	69	$9.1 \times 10^{14}$

radiation spectra from surface SPSs are categorized into broad peaks and sharp peaks, and the radiation wavelengths for each SPS are diverse.<sup>10,13,14</sup> To achieve a better understanding of these phenomena, it is very important to elucidate the defect structure of the surface SPS. However, although an oxygen-related complex has been suggested,<sup>9,15</sup> the specific structure and formation mechanism are still unknown. In previous work, we performed first-principles calculations to derive the HOMO–LUMO gaps of some oxygen-related complexes.<sup>16</sup> We also changed the position of defects with respect to an amorphous-like oxide–SiC interface and precisely reproduced the dispersion in the HOMO–LUMO gap.<sup>16</sup> In the present study, we investigate the radiation properties of surface SPSs and their dependence on the formation process, which is important to verify the cause of the radiation wavelength dispersion for each SPS, and to clarify the defect structure and formation mechanism.

Table I shows the specifications of the substrates used in this study. Here, we have confirmed that most of the surface SPSs formed on these substrates exhibit antibunching characteristics (see [supplementary material](#) for substrates #1–#3 and Ref. 13 for #4). We carried out five types of photoluminescence (PL) measurements for the characterizations of the surface SPSs, i.e.: (i) cryogenic PL measurements, (ii) dependence of radiation properties on substrate surface orientations, (iii) dependence of radiation properties on oxide thickness, (iv) dependence of SPS density on the Ar annealing, and (v) investigation of the Ar annealing for each SPS. Hence, various samples have been fabricated in the experiments. Table II summarizes the sample fabrication processes which were conducted for each experiment.

Cryogenic photoluminescence (PL) measurements were performed to obtain the zero-phonon lines (ZPLs) for each surface SPS. A confocal scanning laser fluorescence microscope (CFM; WITec Inc.) was used for PL measurements. PL spectra were recorded using a spectrometer (Princeton Instruments Inc.) with a CCD detector (Oxford Instruments Inc.). Cryogenic PL measurements were conducted with a liquid nitrogen flow into the sample stage. The second-harmonic wave of a YAG laser (wavelength 532 nm, net input power 1.7 mW) was used as an excitation source.

To verify the cause of wavelength dispersion, the radiation wavelengths for the Si-face were compared with those for the (11–20)  $a$ -

face. In addition to the 4H substrate (#1), a 6H–SiC Si-face homoepitaxial layer (#2) and a 6H–SiC  $a$ -face (#3) were used as substrates. PL measurements of these samples were performed at room temperature using the CFM.

To examine the difference in the radiation properties with the formation process, three types of experiments were conducted: dependence of SPS density and emission energy on the oxide thickness, dependence of SPS density on the Ar annealing temperature, and investigation of the Ar annealing for each surface SPS. In the first experiment, some samples were fabricated with different oxide thicknesses where the oxide thickness was in the range of 1–100 nm, as measured with a spectroscopic ellipsometer. In the second experiment, post-oxidation Ar annealing at the same temperature as oxidation was conducted for a sample with 5 nm oxide thickness. In these two experiments, PL mappings with a 647 nm long-pass filter were performed with an in-house-built CFM.<sup>13</sup> The same CFM system as the cryogenic PL measurements were employed in the third experiment. At least 10 surface SPSs were identified by PL mapping. Ar annealing at various temperatures was performed, and the change in the PL spectra from each SPS due to Ar annealing was traced.

In the cryogenic PL measurements, we identified two types of the PL spectra at 290 K from the surface SPSs, i.e., broad type and sharp type, which was similar to our previous work.<sup>13,15</sup> PL spectra obtained from surface SPSs formed on substrate #1 at various temperatures are shown in Fig. 1. Note that very sharp peaks observed at wavelengths around 555, 565, and between 580 and 590 nm are attributed to the Folded Transvers Optical (FTO) and Folded Longitudinal Optical (FLO) phonon modes, and their second Raman line,<sup>17</sup> respectively. Figures 1(a) and 1(b) show a broad peak at 290 K and a sharp peak at 290 K, respectively. As shown in Fig. 1(a), the radiation predominant to the phonon sideband (PSB) was transformed to a ZPL dominant band with a decrease in the sample temperature. In addition, Fig. 1(b) shows that even if the ZPL is dominant at 290 K, the peak width becomes narrower with a decrease in the temperature.

Figure 2 shows a histogram of ZPL center wavelengths obtained from PL spectra at 80 K for substrate #1. Note that the ZPLs at wavelengths around 555–560 nm and 580–585 nm may not have been counted, because they were obscured by the first or second Raman

TABLE II. Summary of the sample fabrication processes for each experiment.

Experiment	(i)	(ii)	(iii)	(iv)	(v)
Substrate	#1	#1–#3	#4	#4	#1
Oxidation	Dry 800 °C for 5 min	Dry 800 °C for 5 min	Pyrogenic 1100 °C 1–100 nm	Pyrogenic 1100 °C up to 5 nm	Dry 800 °C for 5 min
Ar annealing	800 °C for 5 min	N/A	N/A	1100 °C for 66 min	200–800 °C for 5 min

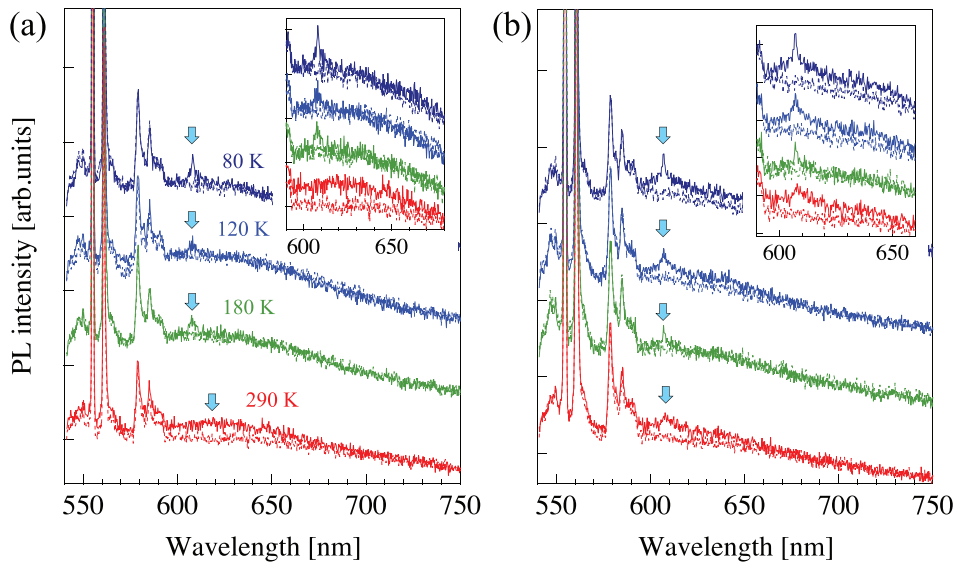


**FIG. 1.** PL spectra from surface SPSs formed on substrate #1 at various temperatures. (a) Broad peak at 290 K, and (b) sharp peak at 290 K. The arrows indicate the center wavelength and the solid and broken lines are spectra from SPS and background (BG), respectively. The measurements were carried out at the temperature from 290 to 80 K. Each spectrum is offset for clarity. The insets show spectra at a wavelength range around emission peak.

line. The histogram shows that the radiation energies are diverse and the energy difference is around 0.33 eV.

According to an *ab initio* study,<sup>16</sup> different local atomic structures give rise to fluctuations of the energy gap, due to the amorphous layer including many stacking faults formed at the oxidized interface. In addition, such a fluctuation was estimated to be 0.33 eV, which is in good agreement with the observed value. Therefore, it is suggested that the variation of wavelength for each surface SPS is due to the relationship between the location of defects and the interfacial amorphous layer. Moreover, the histogram indicates that the radiation energies of the surface SPS are at least 1.88 eV. According to the *ab initio* study,<sup>16</sup>

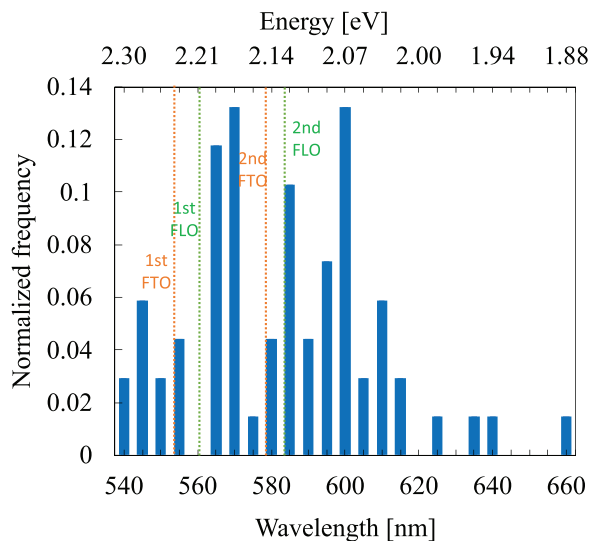


**FIG. 2.** Histogram of ZPL obtained from PL measurements at 80 K for substrate #1. The broken lines in orange and in green represent the positions of the first and second FTO phonon lines and those of the first and second FLO phonon lines, respectively.

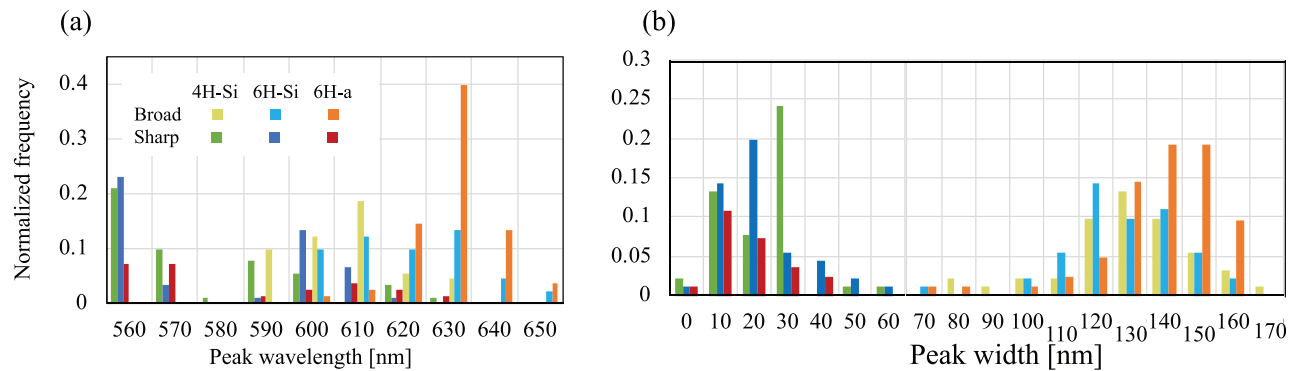
most of the oxygen-related defects form intermediate gap states, of which the HOMO–LUMO gaps over 1.88 eV originate from  $O_{Si}(1)$ ,  $V_{Si}(3)O_C(2)$ ,  $V_C(1)O_{Si}(2)$ , and  $V_C(2)O_{Si}(2)$ . Therefore, these four types of defects are promising candidates for the origin of the surface SPS.

To further verify the cause of wavelength dispersion, we compared the radiation properties of the surface SPSs formed on 4H-SiC (#1), 6H-SiC Si-face (#2), and 6H-SiC *a*-face (#3) substrates. Figures 3(a) and 3(b) show the peak wavelengths and the peak widths (full width at half maximum (FWHMs)) of the surface SPSs for these three samples. Both the peak wavelength and peak width for the 4H- and 6H-SiC Si-faces showed almost the same degree of dispersion. On the other hand, in the case of the *a*-face (6H-SiC), broad peaks were dominant, the center wavelengths were mostly distributed around 630 nm, and the FWHMs were larger than those of the other samples.

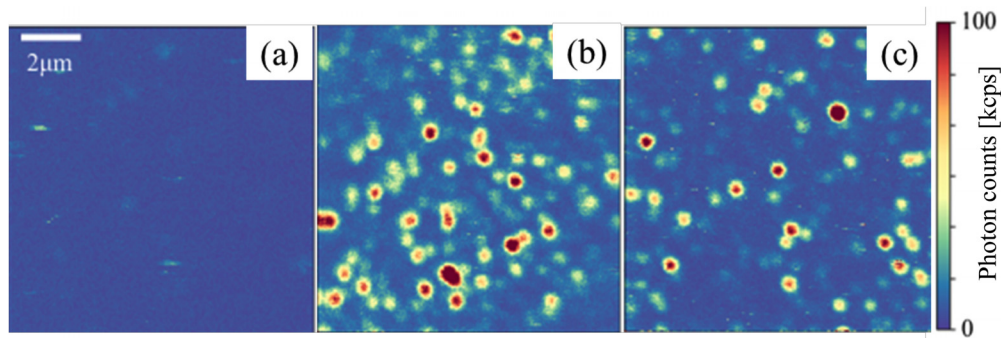
According to an *ab initio* study given, an amorphous layer at the oxide–SiC interface,<sup>16</sup> the dispersion of radiation wavelength is responsible for the energy gap variation due to micro-stacking faults formed at the interface, i.e., such faults cause fluctuation of the conduction band edge of the SiC semiconductor near the surface, so that the energy gap of the SPS becomes variable. No significant difference between Si-faces (4H-SiC, 6H-SiC) was observed and only the dispersion of the *a*-face was small, which can be generally interpreted as indicating that stacking faults are not easily formed on the *a*-face, because the oxidized interface is normal to the stacking fault, which leads to restriction of the conduction band edge fluctuation.

Figure 4 shows PL intensity maps at room temperature for the substrate #4 samples with various oxide thicknesses. Although no SPS was observed in the non-oxidized sample [Fig. 4(a)], the formation of surface SPSs was identified for oxide thicknesses of 1 nm [Fig. 4(b)] and 50 nm [Fig. 4(c)]. Comparison of the 1 nm and 50 nm oxide thicknesses indicated no clear difference in radiation intensity, although the number of surface SPSs significantly decreased with an increase in the oxide thickness.

Figure 5 shows the number of surface SPSs formed in a  $10 \times 10 \mu\text{m}^2$  area as a function of oxide thickness on the #4 substrates. The number of SPSs was almost constant at ca. 90 up to 10 nm; however,



**FIG. 3.** Histograms of radiation properties at room temperature of the surface SPSs on Si-faces (4H- and 6H-SiC) and the a-face (6H-SiC). (a) Peak wavelength and (b) peak width (FWHM).



**FIG. 4.** PL maps at room temperature for the substrate #4 samples with various oxide thicknesses; (a) before oxidation, and for oxide thicknesses of (b) 1 nm and (c) 50 nm.

this then decreased at greater than 10 nm. In addition, with a thicker oxide, the ratio of SPSs that show unstable radiation decreased, which suggests that oxidation over 10 nm thick has both the ability to decrease the density of surface SPSs and to stabilize their radiation.

Figure 6 shows plots of the emission energies measured at room temperature of the surface SPSs in a  $10 \times 10 \mu\text{m}^2$  area for each oxide

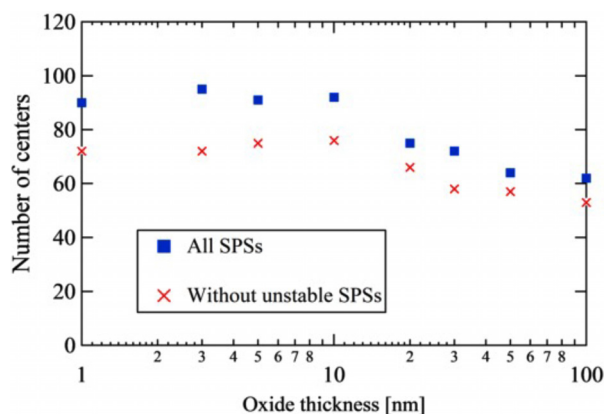


**FIG. 5.** Number of surface SPSs in an area of  $10 \times 10 \mu\text{m}^2$  on the #4 substrate.

thickness on #4 substrates. The minimum photon energies were almost constant at ca. 1.80 eV, while the maximum energy increased with the oxide thickness. However, the average peak energy was constant at ca. 1.84 eV, and thus, no significant change due to oxide thickness was observed. It is probable that the stacking faults at the oxidized interface increased with the oxide thickness, i.e., the heating time, because the strain around the oxide-SiC interface is enhanced, which results in enhancement of the emission energy dispersion.

The effect of Ar annealing on the surface SPSs was investigated. First, the density of the SPSs was compared using the sample with an oxide thickness of 5 nm on the #4 substrate. PL maps at room temperature before and after Ar annealing are shown in Fig. 7. The number of surface SPSs and the radiation intensity were significantly decreased by Ar annealing. The SPS density decreased for oxide thicknesses greater than 10 nm (Fig. 5). This can be explained by considering that a larger oxide thickness corresponds to a longer heating time, which results in a reduction of the SPS density. Therefore, thermal treatment is considered to reduce the number of surface SPSs.

Finally, the impact of Ar annealing on each surface SPS was investigated. Changes in the PL spectra for individual surface SPSs on substrate #1 were traced after Ar annealing at various temperatures. There were many cases in which the radiation intensity was weakened with elevation of the annealing temperature, and such cases comprised 73% of the observed SPSs.

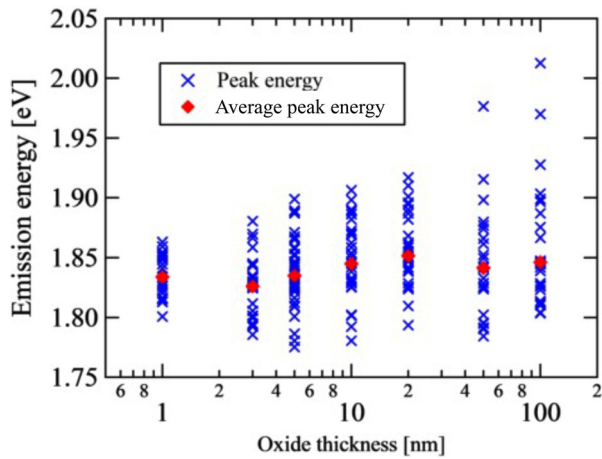


FIG. 6. Emission energy plots measured at room temperature for each oxide thickness on the #4 substrate.

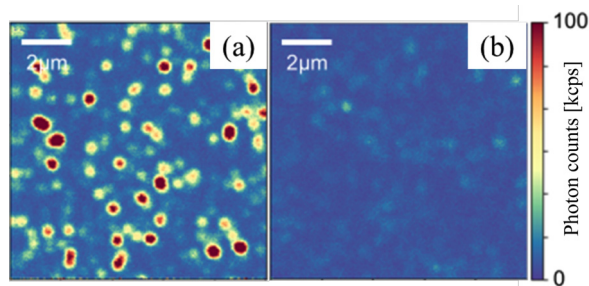


FIG. 7. PL intensity maps at room temperature (a) before and (b) after Ar annealing of the #4 substrates.

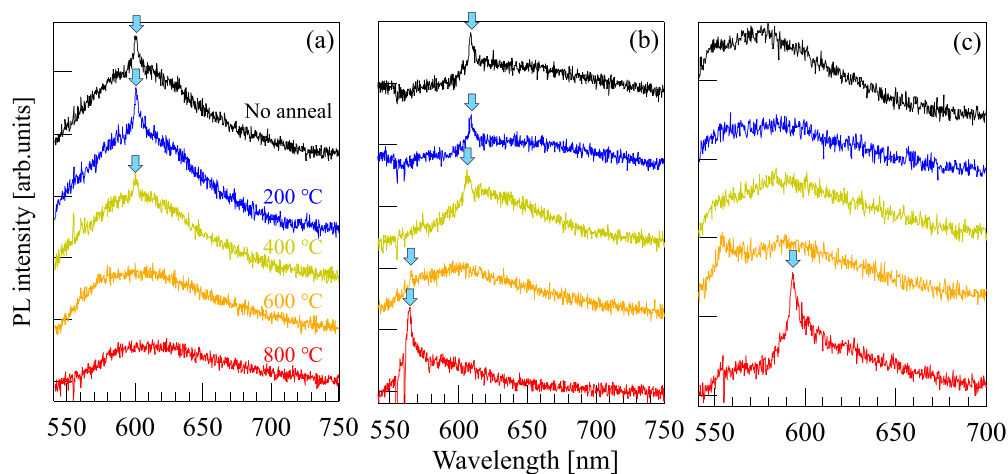


FIG. 8. PL spectra at room temperature for each surface SPS on the #1 substrate after various Ar anneal temperatures: (a) ZPL buried into PSB, (b) ZPL shifted, and (c) the state of SPS changed. BG subtractions were processed. The arrows indicate the center wavelength. Ar annealing was carried out from 200 to 800 °C. Each spectrum is offset for clarity.

On the other hand, there were three other behaviors observed. PL spectra at room temperature for each surface SPS on the #1 substrate after various Ar annealing temperatures are shown in Fig. 8. Figure 8(a) shows that a PL spectrum consisting of ZPL+PSB became only PSB at an annealing temperature of 600 °C, and the intensity was entirely weakened. This case occurred for 19% of the observed SPSs. It is considered that the ratio of PSB was increased by thermal treatment and the radiation itself was weakened. Figure 8(b) shows the case where the ZPL shifted, which occurred for 5% of the observed SPSs. The ZPL around 608 nm disappeared and appeared at 564 nm with an annealing temperature of 600 °C. This wavelength shift, which corresponds to a 0.16 eV shift in photon energy, can be attributed to the structural change of the oxidized interface due to annealing, which results in a change in the radiation energy. Therefore, this demonstrates that a change of the oxidized interface near the surface SPS has an effect on the radiation wavelength shift. Behavior in which the state of SPS itself could be changed is shown in Fig. 8(c). The radiation spectrum was not significantly changed until 600 °C, while a relatively sharp emission peak appeared when annealing at 800 °C. This means that, in addition to the state-change of the oxidized interface, a change that has an effect of PSB elimination occurred in the surface SPS itself. To summarize, Ar annealing was determined to enhance the changes of state in the oxidized interface and the surface SPS, which resulted in changes of the wavelength shift and PSB generation rate, respectively.

Changes in the radiation properties due to Ar annealing typically occurred at an annealing temperature of 600 °C; therefore, we discuss the meaning of this temperature. According to Johnson *et al.*,<sup>18</sup> post-oxidation NO annealing has an effect on the density of SPSs as well as a reduction of the interface state density. Therefore, the formation of metal oxide semiconductor (MOS) interface defects may be correlated with that of surface SPSs. In our previous work, Ar annealing also has an effect on the change of the MOS interface characteristics and the oxygen-related structural change.<sup>19</sup> Furthermore, the annealing temperature that induced these changes was 600 °C. Therefore, it is inferred that the interface states in the MOS characteristics and the

generation of surface SPSs are closely related to each other, and their structural change requires a heating temperature of 600 °C or more.

According to Ref. 19, O 2p spectra obtained using ultraviolet photoemission spectroscopy were changed at 600 °C, which was attributed to a reduction of the O atom density at the oxide–SiC interface and inferred that O atoms at the interface begin to move at this annealing temperature. In density functional theory (DFT) calculations,<sup>20</sup> the migration-energy barrier of an O atom at the SiC surface was ca. 0.9 eV. We estimated the event frequency of such O atom displacement to have an energy barrier of 0.9 eV at an annealing temperature of 600 °C. Given the assumption that the oscillation frequency of O atoms at the SiC surface corresponds to the optical phonon of Si, the event frequency was a few events per second. Therefore, this result could indicate that a structure change of the surface SPSs occurs at 600 °C and the changes in their radiation properties originate from the displacement of O atoms as a part of the surface SPSs.

In this study, we obtained knowledge on the radiation properties and dependency of surface SPSs on the formation processes. Low temperature PL measurements revealed that ZPL solely appears at low temperatures and the emission energies of ZPL had a 0.33 eV dispersion for each surface SPS. Comparison of the radiation properties between the Si-face and *a*-face suggested that fewer stacking faults were formed at the oxidized interface on *a*-face; therefore, the dispersion of emission energies was restricted. These results revealed that stacking faults formed near the oxidized interface can be responsible for the emission energy dispersion of the surface SPSs, which has been suggested from our *ab initio* simulations. In addition, the precise ZPL energies obtained from low temperature PL measurements inferred several defect structures as the origin of the surface SPS. The dependence of the SPS formation density and emission energies of the surface SPSs on the oxide thickness indicated that as the oxide thickness increases, the number of unstable SPSs is reduced, although the total number of SPSs is also reduced, and the emission energy dispersion is enhanced. We infer that this energy dispersion is attributed to an increase in the stacking faults due to the enhancement of strain around the oxide–SiC interface. The formation density of surface SPS formed was reduced with elevation of the Ar anneal temperature, which suggests that thermal treatment has an ability to reduce the surface SPSs. Furthermore, PL spectra were measured for each surface SPS after various Ar annealing temperatures. As a result, a ZPL shift, a reduction in radiation intensity, and a change of the state of SPSs were observed at an annealing temperature of 600 °C. Finally, experimental and theoretical studies suggested that the structural change of the surface SPSs at this temperature originates from the displacement of O atoms at the oxide–SiC interface.

See the [supplementary material](#) for second-order correlation functions ( $g^2(\tau)$ ) obtained from surface SPSs on 4H-SiC Si-face (substrate #1), 6H-SiC Si-face (substrate #2), and *a*-face (substrate #3) substrates.

This work was supported in part by Grants-in-Aid for Scientific Research (Nos. 18H03770 and 20H00355) from the Japan Society for the Promotion of Science (JSPS).

## DATA AVAILABILITY

The data that support the findings of this study are available from the corresponding author upon reasonable request.

## REFERENCES

- <sup>1</sup>F. Fuchs, V. A. Soltamov, S. Vāth, P. G. Baranov, E. N. Mokhov, G. V. Astakhov, and V. Dyakonov, *Sci. Rep.* **3**, 1637 (2013).
- <sup>2</sup>D. Fattal, E. Diamanti, K. Inoue, and Y. Yamamoto, *Phys. Rev. Lett.* **92**, 037904 (2004).
- <sup>3</sup>N. Mizuochi, T. Makino, H. Kato, D. Takeuchi, M. Ogura, H. Okushi, M. Nothhaft, P. Neumann, A. Gali, F. Jelezko, J. Wrachtrup, and S. Yamasaki, *Nat. Photonics* **6**, 299 (2012).
- <sup>4</sup>M. Widmann, S.-Y. Lee, T. Rendler, N. T. Son, H. Fedder, S. Paik, L.-P. Yang, N. Zhao, S. Yang, I. Booker, A. Denisenko, M. Jamali, S. A. Momenzadeh, I. Gerhardt, T. Ohshima, A. Gali, E. Janzén, and J. Wrachtrup, *Nat. Mater.* **14**, 164 (2015).
- <sup>5</sup>H. Kraus, D. Simin, C. Kasper, Y. Suda, S. Kawabata, W. Kada, T. Honda, Y. Hijikata, T. Ohshima, V. Dyakonov, and G. V. Astakhov, *Nano Lett.* **17**, 2865 (2017).
- <sup>6</sup>T. Ohshima, T. Satoh, H. Kraus, G. V. Astakhov, V. Dyakonov, and P. G. Baranov, *J. Phys. D: Appl. Phys.* **51**, 333002 (2018).
- <sup>7</sup>D. J. Christle, A. L. Falk, P. Andrich, P. V. Klimov, J. Ul Hassan, N. T. Son, E. Janzén, T. Ohshima, and D. D. Awschalom, *Nat. Mater.* **14**, 160 (2015).
- <sup>8</sup>S. Castelletto, B. C. Johnson, V. Ivády, N. Stavrias, T. Umeda, A. Gali, and T. Ohshima, *Nat. Mater.* **13**, 151 (2014).
- <sup>9</sup>A. Lohrmann, S. Castelletto, J. R. Klein, T. Ohshima, M. Bosi, M. Negri, D. W. M. Lau, B. C. Gibson, S. Praver, J. C. McCallum, and B. C. Johnson, *Appl. Phys. Lett.* **108**, 021107 (2016).
- <sup>10</sup>A. Lohrmann, N. Iwamoto, Z. Bodrog, S. Castelletto, T. Ohshima, T. J. Karle, A. Gali, S. Praver, J. C. McCallum, and B. C. Johnson, *Nat. Commun.* **6**, 7783 (2015).
- <sup>11</sup>S.-i Sato, T. Honda, T. Makino, Y. Hijikata, S.-Y. Lee, and T. Ohshima, *ACS Photonics* **5**, 3159 (2018).
- <sup>12</sup>Y. Abe, T. Umeda, M. Okamoto, R. Kosugi, S. Harada, M. Haruyama, W. Kada, O. Hanaizumi, S. Onoda, and T. Ohshima, *Appl. Phys. Lett.* **112**, 031105 (2018).
- <sup>13</sup>H. Tsunemi, T. Honda, T. Makino, S. Onoda, S.-I. Sato, Y. Hijikata, and T. Ohshima, *Mater. Sci. Forum.* **924**, 204 (2018).
- <sup>14</sup>B. Lienhard, T. Schröder, S. Mouradian, F. Dolde, T. T. Tran, I. Aharonovich, and D. Englund, *Optica* **3**, 768 (2016).
- <sup>15</sup>Y. Hijikata, T. Horii, Y. Furukawa, Y.-i Matsushita, and T. Ohshima, *J. Phys. Commun.* **2**, 111003 (2018).
- <sup>16</sup>Y.-i Matsushita, Y. Furukawa, Y. Hijikata, and T. Ohshima, *Appl. Surf. Sci.* **464**, 451 (2019).
- <sup>17</sup>J. C. Burton, L. Sun, F. H. Long, Z. C. Feng, and I. T. Ferguson, *Phys. Rev. B* **59**, 7282 (1999).
- <sup>18</sup>B. C. Johnson, J. Woerle, D. Haasmann, C. T.-K. Lew, R. A. Parker, H. Knowles, B. Pingault, M. Atature, A. Gali, S. Dimitrijević, M. Camarda, and J. C. McCallum, *Phys. Rev. Appl.* **12**, 044024 (2019).
- <sup>19</sup>Y. Hijikata, H. Yaguchi, S. Yoshida, Y. Ishida, and M. Yoshikawa, *J. Vac. Sci. Technol. A* **23**, 298 (2005).
- <sup>20</sup>Y.-I. Matsushita and A. Oshiyama, [arXiv:1612.00189v1](#) (2016).